Hindawi
International Journal of RF and Microwave Computer-Aided Engineering
Volume 2023, Article ID 6496757, 8 pages
https://doi.org/10.1155/2023/6496757

Research Article

A Flexible Multiband Dendritic Structure Fractal Antenna for 4G/5G/WLAN/Bluetooth Applications

Zhen Yu,[1] **Guodong Zhang**,[1] **Xiaoying Ran**,[1] **Ruirong Niu**,[1] **Runzhi Sun**,[1] **Ziheng Lin**,[1] **and Zewei Lu**[2]

[1]*North China Institute of Science and Technology, Beijing 101601, China*
[2]*Institute of Disaster Prevention, Beijing 101601, China*

Correspondence should be addressed to Xiaoying Ran; starsky202@ncist.edu.cn

Received 21 March 2023; Revised 3 August 2023; Accepted 11 August 2023; Published 31 August 2023

Academic Editor: Piotr Gas

In this study, a flexible multiband fractal antenna mimicking dendrite structure is proposed and designed by combining bionics and fractal theory. The dendritic structure of neurons is extracted and simplified into a simple and clear geometric structure. The initial antenna model is obtained by fractal operation on the geometric structure, and finally, four effective bands are obtained. The antenna is printed on a $50^{*}70^{*}0.1\,mm^{3}$ polyimide dielectric board and fed by a coplanar waveguide. This paper discusses the effect of the human body on the performance of the antenna and the robustness of the antenna in the bending regime. The gain, efficiency, and cross-polarization of the antenna were tested using a microwave anechoic chamber. The measured antenna covers 1.37 GHz-1.93 GHz (relative bandwidth 35%), 2.25 GHz-2.51 GHz (relative bandwidth 10.7%), 3.13 GHz-3.81 GHz (relative bandwidth 19.3%), and 4.46 GHz-5.5 GHz (relative bandwidth 21.1%) four operating frequency bands. The maximum gain is 6.05 dBi and the maximum efficiency is 91.05%. The antenna can be used for Bluetooth WLAN (Wireless Local Area Network), 4G (4th Generation Communication System), 5G (5th Generation Mobile Communication System), WiMAX (Worldwide Interoperability for Microwave Access), etc. The test results are in good agreement with the simulation results, which proves that the antenna can meet various wireless communication requirements.

1. Introduction

With the continuous progress of electronic technology, in order to better meet the needs of people, the frequency bands that electronic equipment needs to cover are increasing, so the demand for high-performance multiband antennas is also increasing. And to give enough room for other hardware in electronic devices, some researchers have focused their efforts on flexible conformal antennas. Moreover, the robustness of flexible antenna when it is bent has attracted more attention.

In order to achieve the multiband effect, engineers have developed a series of technical solutions, such as slot loading technology [1], coupled feeding technology [2], matching loading technology, and frequency doubling technology. These techniques have been published in a large number of papers as solutions to multiband techniques [3, 4]. In article [5], the method of eigenmode analysis was used to nest the circle and triangle to design an antenna that can cover 3G, 4G, 5G, and other communication frequency bands, and good performance was obtained. Similar antennas such as [6] have obtained good performance using similar design ideas. And through people's exploration and discovery, applying fractal technology to antenna design using unequal branches can produce the effect of multiple frequency points. For example, in [7], the authors adopted the traditional Chinese cloud image as the base model and used the slotted technique and fractal nesting to obtain the multiband

Table 1: Performance comparison of the proposed antenna with recent pioneering state of arts.

Ref.	Size (mm^3)	Res. freq. (GHz)	Gain (dBi)	Dielectric material
6	80*80*3.175	1.56/2.49/3.5/5.24	3.49/6.49/4.93/4.46	Rogers AD255C
7	35*40*0.635	2.35/3.65/5.6	3.26/2.92/4.14	FR-4
9	19.5*17.6	1.3/2.44/3.5	0.93, 4.98, 2.71	FR-4
14	60*45*0.125	1.9/6.2/10.5	—	Paper
18	40*50*1.6	1.7/2.4/3.8/5.4	4.63/3.42/4.24	FR-4
20	41*29*1.6	1.7/3.6/5	2.41/3.86/3.91	FR-4
Prop.	50*70*0.1	1.6/2.41/3.52/4.92	2.12/3.95/4.26/6.05	Polyimide

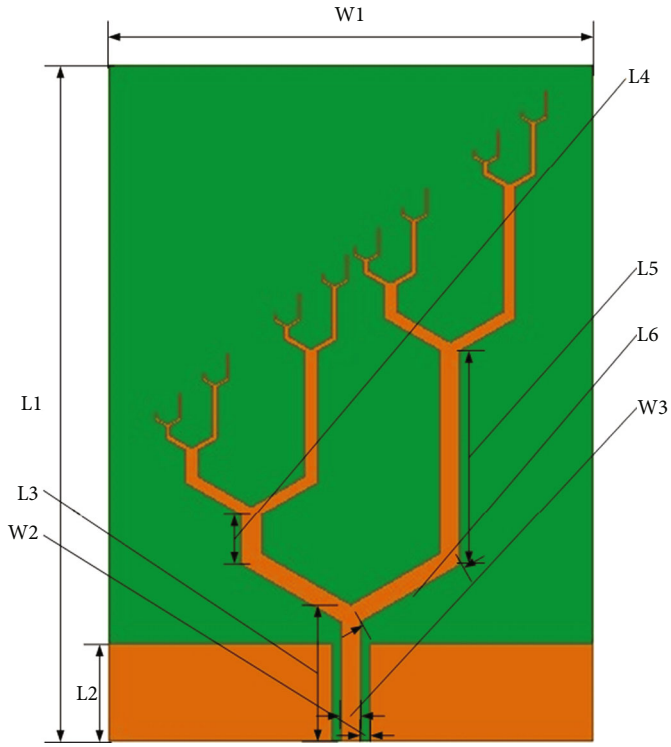

Figure 1: Antenna structure layout.

Table 2: The dimensions of the proposed antenna design.

Dimension parameters	L1	L2	L3	L4	L5
Unit (mm)	70	10	14	3.6	23
Dimension parameters	W1	W2	W3	L6	
Unit (mm)	50	1	2	13	

response of the antenna. In addition, different feeding methods have a great impact on the performance of the antenna. The coplanar waveguide feeding method produces excellent dispersion characteristics due to the continuous magnetic field interaction between the transmission line and the ground plane, which can expand the bandwidth to a certain extent [8, 9]. The antenna fed by microstrip line has a relatively narrow width due to its microstrip line mode [10].

For flexible antennas, it is very important to maintain stable performance when deformation or other external conditions change to a certain extent. However, different dielectric materials affect the performance and frequency band coverage of the antenna to a certain extent due to their different dielectric constant and loss tangent values [11–13].

In [14], the authors tried to use paper as a dielectric material and used conductive silver paste to make radiators and achieved good results. However, due to the limitations of paper itself, including its fragile nature and the instability of its dielectric constant after being exposed to moisture, paper was not a good dielectric material, but this attempt was still a successful attempt. In literature [15], the authors used leather as the dielectric material for related attempts, and felt was used as the dielectric material in [16], both of which have relatively good performance.

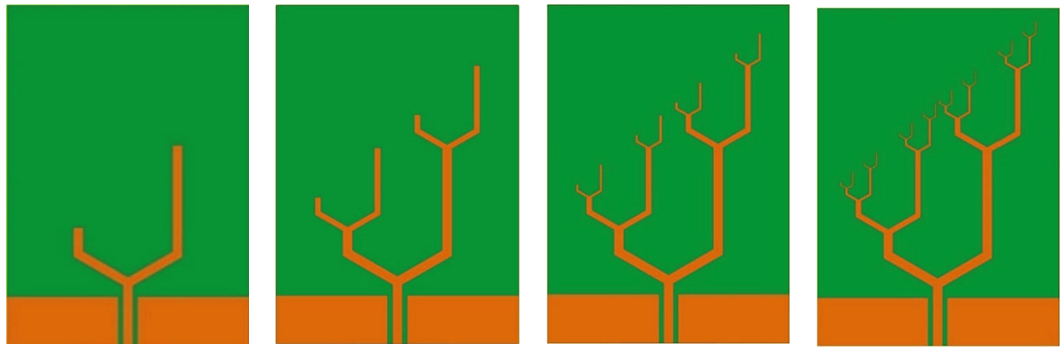

Figure 2: Fractal evolution of antennas: (a) 0th iteration; (b) 1st iteration; (c) 2nd iteration; (d) 3rd iteration.

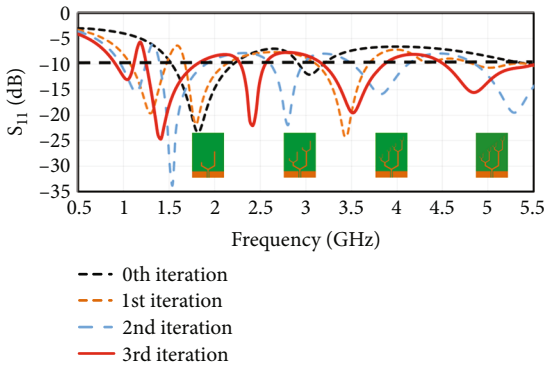

Figure 3: S11 comparison diagram of antenna-nested iteration.

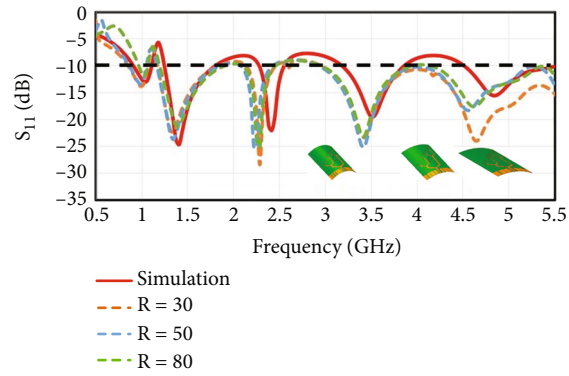

Figure 4: Antenna conformal bend S11 comparison.

In the continuous exploration of antenna technology, people try to apply fractal and bionic theory to antenna design [17]. For example, in [18], the authors fabricated a coplanar waveguide antenna mimicking antlers, which realized the multiband response of the antenna by using the asymmetry of antlers and the structure of branches. In [19], the authors made a planar Vivaldi antenna inspired by the growth state of ferns by using the principle of bionics and obtained considerable results. In [20], the authors combined bionics and fractal to subtype and nest the semiring structure and fabricated a chrysanthemum-shaped coplanar waveguide antenna with remarkable effect.

In this paper, a flexible antenna simulating the fractal structure of dendritic is proposed and designed by combining the principles of bionics and fractal. The multiband effect is generated in the continuous subdivision iteration. The antenna has good radiation performance and can be used in Bluetooth WLAN, 4G, 5G, WiMAX, and other applications. Compared with the traditional multiband method, due to the high self-similarity of the structure of the antenna, the required band combination of the product can be obtained by increasing or decreasing the number of fractal iterations without changing the overall structure of the antenna.

The performance comparison between the antenna proposed in this paper and the antenna in the reference is shown in Table 1. The antenna proposed in this paper uses fractal and bionic technology to achieve the characteristics of multiband, relatively high gain and relatively high efficiency.

2. Structural Characteristics of the Antenna

The structure schematic of the proposed fractal antenna with a dendritic-like structure is shown in Figure 1, and its size parameters are shown in Table 2. The antenna is printed on a polyimide substrate with a thickness of 0.1, a dielectric constant ε_r of 3.5, and a loss tangent of 0.008.

The 0th iteration model of the antenna is based on a structure similar to a Y-shaped branch, where the angle of the V-shaped structure is 120°. The 1st iteration, 2nd iteration, and 3rd iteration fractals scale the V structure in the 0th iteration model in different proportions. The relationship between the size of the branch in each iteration and the size of the previous iteration is shown in

$$D_n = \left(\frac{3}{20}n^2 - \frac{13}{20}n + 1.1\right)D_{n-1}. \quad (1)$$

In the formula, D_n represents the size of the new branch at the nth iteration. Figure 2 shows the fractal evolution process of the antenna.

As a traditional monopole antenna, the relationship between the electrical length of the antenna and the frequency can be calculated using

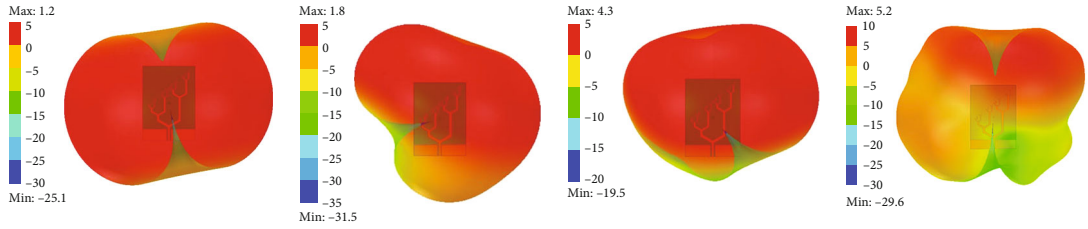

FIGURE 5: Antenna 3D far-field radiation direction diagram: (a) 1.41 GHz; (b) 2.41 GHz; (c) 3.52 GHz; (d) 4.85 GHz.

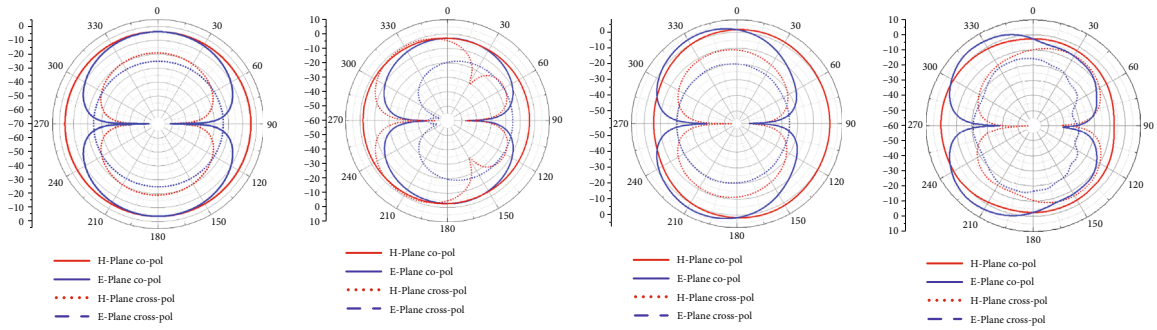

FIGURE 6: Cross-polarization and coplanar polarization in the E/H-plane of the antenna: (a) 1.41 GHz; (b) 2.41 GHz; (c) 3.52 GHz; (d) 4.85GHz.

$$
\begin{aligned}
f &= \frac{c}{2L\sqrt{\varepsilon_r}},\\
L_a &= (L_6 + L_4) + (L_3 - L_2) + \sum_{n=1}^{n=3}\left\{(L_6 + L_5) * \left(\frac{3}{20}n^2 + \frac{13}{20}n + 1.1\right)\right\} \approx 54\,\text{mm},\\
f_a &= \frac{c}{2L_a\sqrt{\varepsilon_r}} \approx 1.46\,\text{GHz},\\
L_b &= \frac{3(L_6 + L_5)}{5} + \frac{6(L_6 + L_5)}{25} + \frac{3(L_6 + L_5)}{25} \approx 34.5\,\text{mm},\\
f_b &= \frac{c}{2L_b\sqrt{\varepsilon_r}} \approx 2.41\,\text{GHz},\\
L_c &= \frac{3(L_6 + L_4)}{5} + \frac{6(L_6 + L_4)}{25} \approx 24\,\text{mm},\\
f_c &= \frac{c}{2L_c\sqrt{\varepsilon_r}} \approx 3.47\,\text{GHz},\\
L_d &= L_4 + \frac{3(L_6 + L_4)}{5} + \frac{6(L_6)}{25} \approx 16.7\,\text{mm},\\
f_d &= \frac{c}{2L_d\sqrt{\varepsilon_r}} \approx 4.8\,\text{GHz},
\end{aligned}
\tag{2}
$$

where f_a, f_b, f_c, and f_d represent the central frequency points of the four main frequency bands of the antenna and L_a, L_b, L_c, and L_d represent the electrical length of the corresponding frequency points.

3. Simulation Results

Figure 3 shows the comparison of S11 for different numbers of iterations during the antenna evolution. The antenna can be considered as a monopole antenna with a capacitive load. The HFSS simulation of the 0th iteration of the model shows that the antenna produces two frequency points corresponding to the two branches of the antenna. As the number of iterations increases, the number of frequency bands generated by the antenna increases and reaches a maximum at the 2nd iteration. The 3rd iteration obtains a completely different combination of frequency bands from the 2nd iteration, so the antenna application personnel can choose different iterations to use according to their needs. Since the 3rd iteration covers more commercial bands, the 3rd iteration is used as the main iteration for the subsequent analysis.

The antenna was coformed with cylinders of radius 30 mm, 50 mm, and 80 mm, respectively, and the comparison of the performance change of the antenna after conformal analysis is done by simulation. Its S11 comparison diagram is shown in Figure 4. It can be seen that the bending has a weak effect on the frequency band of this antenna at low frequencies but makes the frequency point above 2 GHz shift to the left and produces a broadband tendency in the 3 GHz-5.5 GHz band. The coverage bands change from 1.24 GHz-1.8 GHz, 2.29 GHz-2.55 GHz, 3.20 GHz-3.85 GHz, and 4.53 GHz-5.5 GHz to 1.18 GHz-1.8 GHz, 2.12 GHz-2.45 GHz, and 2.97 GHz-5.5 GHz. The above experiments have verified that the antenna has strong robustness in bending.

The 3D far-field radiation direction diagram of the dendritic antenna is shown in Figure 5. The directionality of the antenna becomes stronger as the frequency of each resonant point of the antenna increases. The peak gain at resonance points 1.41 GHz, 2.41 GHz, 3.52 GHz, and 4.85 GHz are 1.2 dBi, 1.8 dBi, 4.3 dBi, and 5.2 dBi. The coplanar polarization and cross-polarization of the E/H-plane are shown in

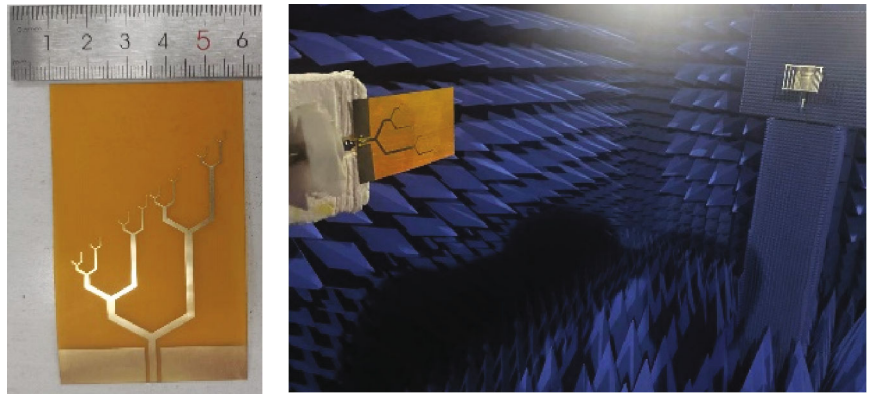

(a) (b)

Figure 7: (a) The antenna prototype. (b) The antenna is tested in an electromagnetically shielded darkroom.

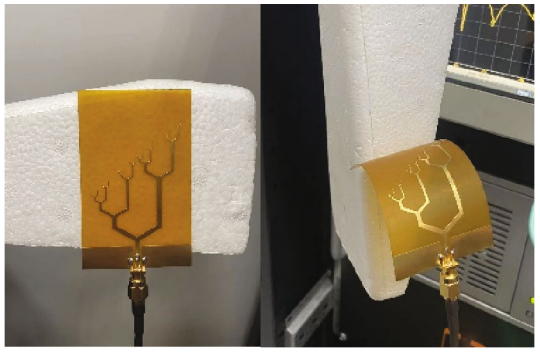

Figure 8: Plot of planar versus curved antenna in S11 test.

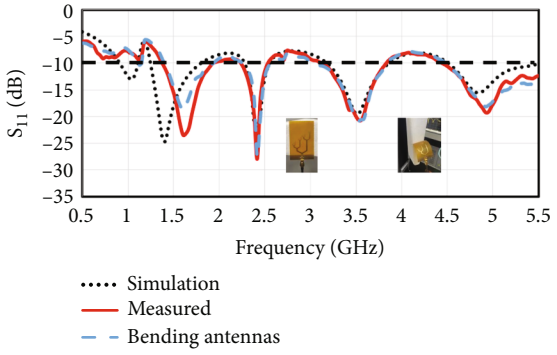

Figure 9: Comparison between actual antenna bending and simulation S11.

Figure 6 The maximum isolation between the coplanar polarization and the corresponding cross-polarization of the antenna at each resonant frequency point is greater than -20 dB, so the radiation performance of the antenna at each frequency point is good.

4. Fabrication and Measured Results

The dielectric plate of the antenna prototype is made of 70*50 mm polyimide with a thickness of 0.1 mm. Polyimide is an excellent dielectric material due to its corrosion resistance and stable electrical properties.

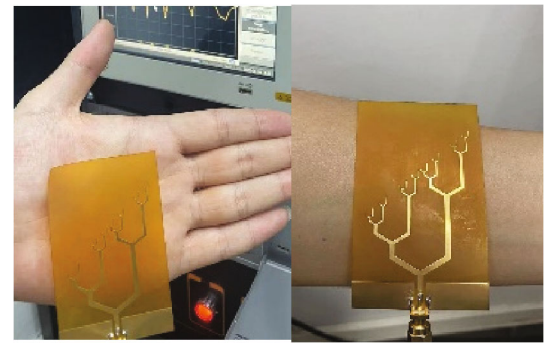

Figure 10: S11 schematic representation of the antenna placed on the middle of the forearm and palm during the test.

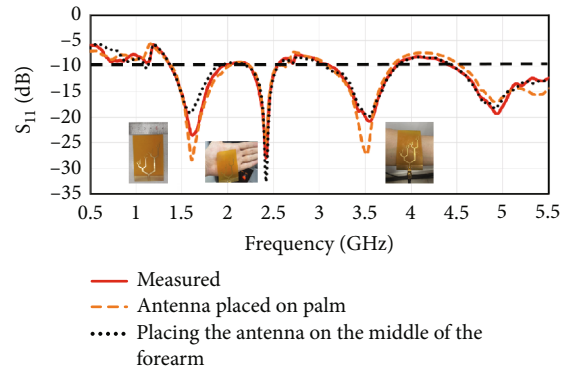

Figure 11: Comparison of the S11 values when the antenna is placed on different parts of the human body.

Figure 7 shows an image of the prototype antenna and the antenna being placed into the antenna test system for testing. The antenna test system consists of an electrically shielded darkroom, a high precision turntable, an antenna probe, and associated test software. The S11 diagram of the antenna was tested with a vector network analyzer, the Agilent E5071B.

The bent antenna line is tested against the S11 of the planar antenna as shown in Figure 8. Figure 9 shows the comparison of the bent antenna with the simulated S11 of the flat antenna. Compared with the simulated antenna, S11 in the

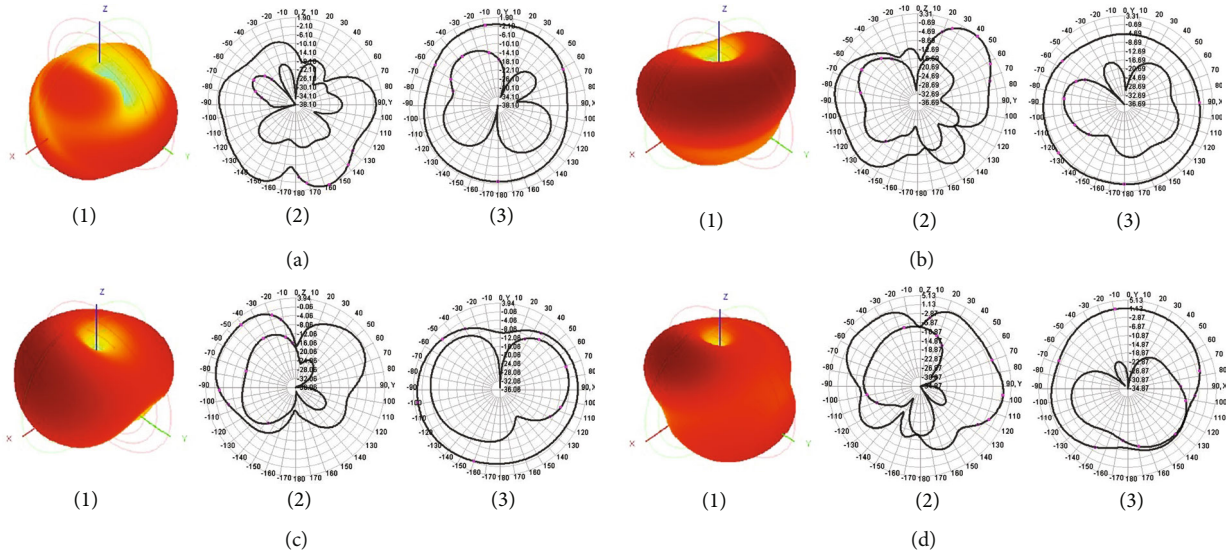

Figure 12: (1) 3D far-field radiation pattern of the antenna, (2) E-plane co-pol and cross-pol comparison diagram, and (3) H-plane co-pol and cross-pol comparison diagram: (a) 1.6 GHz; (b) 2.41 GHz; (c) 3.52 GHz; (d) 4.92 GHz.

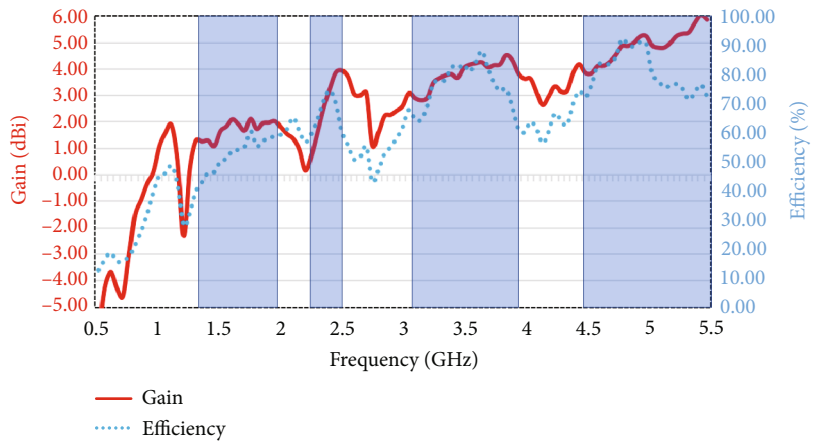

Figure 13: The measured gain and efficiency of the antenna.

first band is shifted from 1.24 GHz-1.8 GHz to 1.37 GHz-1.93 GHz, and the center frequency is shifted from 1.41 GHz to 1.6 GHz. S11 in the third center frequency point is shifted from 4.85 GHz to 4.92 GHz. When analyzing the effect of antenna bending, it is found that the bending in the low frequency band changes the S11 from -23.4 dB to -18.7 dB, but otherwise, the bending has no significant effect on the S11 value in the band and other frequency bands of the antenna, which indicates that the antenna has good robustness in bending.

Figure 10 shows the antenna placed on the middle of the forearm and the palm of the hand during the S11 test. Figure 11 shows the comparison of the S11 values when the antenna is placed on different parts of the human body, and it can be seen that the S11 values of the antenna change to different degrees by this operation. When the antenna is placed on the hand, the first frequency point S11 value changes from -23.4 dB to -28.4 dB, and the third frequency point S11 value changes from -20.7 dB to -27.2 dB; when the antenna is placed on the middle of the forearm, the first frequency point S11 value changes from -23.4 dB to -19.1 dB, and the second frequency point changes from -27.9 dB to -32.6 dB. The reason for the change in S11 value may be related to the absorption of radiation by the human body and the corresponding induced electric field. The change of S11 value when the antenna is placed on different parts of the body may be due to the different thickness of skin, fat, muscle, and bone in different parts of the body.

Figure 12 (1) is the 3D far-field radiation pattern of the antenna at each frequency point, Figure 12 (2) is the coplanar polarization and cross-polarization diagram of the antenna at each frequency point in the E-plane, and Figure 12 (3) is the coplanar polarization and cross-polarization diagram of the antenna at each frequency point in the H-plane. In analysis (1), we can find that the overall radiation direction of the antenna tends to omnidirectional radiation; in analyses (2) and (3), we can see that the maximum isolation degree of cross-polarization and coplanar

polarization of each frequency point of the antenna is above -30 dB to meet the requirements of coplanar polarization and cross-polarization isolation degree of the antenna.

Figure 13 shows the measured gain and efficiency of the antenna, where the red solid line is the measured gain of the antenna and the blue dashed line is the measured efficiency of the antenna. From this picture, it can be seen that the gain of the antenna in the first band is 1.26 dBi-2.12 dBi, and the efficiency is 43%-60.4%. The gain of the second band is 0.74 dBi-3.95 dBi, with an efficiency of 59.6%-71%, covering a variety of important commercial applications such as Bluetooth and WLAN. The third band has a gain of 2.83 dBi-4.26 dBi and an efficiency of 64.4%-88%, covering a number of important mobile communication bands such as 5G band n78, WiMAX, and LTE 42/43. The fourth band has a gain of 3.85 dBi-6.05 dBi and an efficiency of 72.14%-91.05%, covering the 5G band of the WLAN, and the 4.94-4.99 GHz band was suggested at the WRC03 conference for emergency and public protection applications. This antenna may play an active role in the future in the field of emergency and public protection.

5. Conclusion

This design proposes a multiband fractal antenna with imitation dendrite structure. The antenna covers GPS, BDS (Beidou Navigation Satellite System), 4G, 5G, Bluetooth, WLAN, WiMAX, and other frequency bands, covering 1.37 GHz-1.93 GHz, 2.25 GHz-2.51 GHz, 3.13 GHz-3.81 GHz, and 4.46 GHz-5.5 GHz, with corresponding relative band widths of 35%, 10.7%, 19.3%, and 21.1%. If -6 dB is selected as the S11 standard for the antenna, the antenna can be regarded as a broadband antenna, and since the antenna polarization method is line polarization, the availability of the satellite positioning system band it covers is to be explored.

Data Availability

The simulation and test data used to support the findings of this study are included within the figure files.

Conflicts of Interest

The authors declare that there are no conflicts of interest. There is no conflict of interest with the coauthors.

Acknowledgments

This work was supported in part by the Natural Science Foundation of Hebei Province (no. F2021508009), the National Key R&D Project (no. 2020YFC1511805), the S&T Program of Hebei (22375411D), and the Fundamental Research Funds for the Central Universities (3142023058).

References

[1] R. K. Yadav, J. Kishor, and R. L. Yadava, "A Chaucer microstrip fractal antenna for mobile applications," *Journal of Communications Technology and Electronics*, vol. 61, no. 2, pp. 138–144, 2016.

[2] J. Y. Deng, J. Yao, and L. X. Guo, "Compact multiband antenna for mobile terminal applications," *Microwave and Optical Technology Letters*, vol. 60, no. 7, pp. 1691–1696, 2018.

[3] M. J. Jeong, N. Hussain, H.-U. Bong et al., "Ultrawideband microstrip patch antenna with quadruple band notch characteristic using negative permittivity unit cells," *Microwave and Optical Technology Letters*, vol. 62, no. 2, pp. 816–824, 2020.

[4] J. Park, M. Jeong, N. Hussain, S. Rhee, P. Kim, and N. Kim, "Design and fabrication of triple-band folded dipole antenna for GPS/DCS/WLAN/WiMAX applications," *Microwave and Optical Technology Letters*, vol. 61, no. 5, pp. 1328–1332, 2019.

[5] D. H. Patel and G. D. Makwana, "Multiband antenna for GPS, IRNSS, Sub-6 GHz 5G and WLAN applications," *Progress in Electromagnetics Research M*, vol. 116, pp. 53–63, 2023.

[6] D. H. Patel and G. D. Makwana, "Multiband antenna for 2G/3G/4G and sub-6 GHz 5G applications using characteristic mode analysis," *Progress In Electromagnetics Research M*, vol. 115, pp. 107–117, 2023.

[7] Z. Yu, G. Zhang, X. Ran, Z. Lin, and Y. Li, "A cloud-structured fractal multiband antenna for 4G/5G/WLAN/Bluetooth applications," *International Journal of Antennas and Propagation*, vol. 2022, Article ID 1270271, 10 pages, 2022.

[8] A. Kumar, V. Sankhla, J. K. Deegwal, and A. Kumar, "An offset CPW-fed triple-band circularly polarized printed antenna for multiband wireless applications," *AEU-International Journal of Electronics and Communications*, vol. 86, pp. 133–141, 2018.

[9] F. Fertas, K. Fertas, T. A. Denidni, and M. Challal, "Design of miniaturized tri-band antenna based on differential evolution algorithm," *Microwave and Optical Technology Letters*, vol. 65, no. 3, pp. 930–935, 2023.

[10] Z. Yu, J. Yu, X. Ran, and C. Zhu, "A novel ancient coin-like fractal multiband antenna for wireless applications," *International Journal of Antennas and Propagation*, vol. 2017, Article ID 6459286, 10 pages, 2017.

[11] Y. Song, D. Le Goff, and K. Mouthaan, "Highly flexible and conformal 2x2 antenna array on RTV silicone for the 2.4 GHz ISM band," in *2020 IEEE International Symposium on Antennas and Propagation and North American Radio Science Meeting*, Montreal, QC, Canada, 2021.

[12] A. T. Castro and S. K. Sharma, "Inkjet-printed wideband circularly polarized microstrip patch array antenna on a PET film flexible substrate material," *IEEE Antennas and Wireless Propagation Letters*, vol. 17, no. 1, pp. 176–179, 2018.

[13] R. B. Simorangkir, Y. Yang, L. Matekovits, and K. P. Esselle, "Dual-band dual-mode textile antenna on PDMS substrate for body-centric communications," *IEEE Antennas and Wireless Propagation Letters*, vol. 16, pp. 677–680, 2017.

[14] H. A. Elmobarak, S. K. A. Rahim, M. Himdi, X. Castel, and T. A. Rahman, "Low cost instantly printed silver nano ink flexible dual-band antenna onto paper substrate," in *IEEE 2017 11th European Conference on Antennas and Propagation*, Paris, France, 2017.

[15] B. B. Q. Elias, P. J. Soh, A. A. Al-Hadi, and P. Akkaraekthalin, "Gain optimization of low-profile textile antennas using CMA and active mode subtraction method," *IEEE Access*, vol. 9, pp. 23691–23704, 2021.

[16] S. Pujayita, M. Debasis, and K. Susanta, "Control of gain and SAR for wearable antenna using AMC structure," *Radioengineering*, vol. 30, no. 1, pp. 81–88, 2021.

[17] Y. Shi, X. Zhang, Q. Qiu, Y. Gao, and Z. Huang, "Design of terahertz detection antenna with fractal butterfly structure," *IEEE Access*, vol. 9, pp. 113823–113831, 2021.

[18] Y. Li, Y. Zhen, T. Xie, Y. Jianguo, L. Wang, and X. Gao, "A novel binary branch bionic antenna for communication and navigation," *International Journal of RF and Microwave Computer-Aided Engineering*, vol. 32, no. 4, article e23037, 2022.

[19] B. Biswas, R. Ghatak, and D. R. Poddar, "A fern fractal leaf inspired wideband antipodal Vivaldi antenna for microwave imaging system," *IEEE Transactions on Antennas and Propagation*, vol. 65, no. 11, pp. 6126–6129, 2017.

[20] Z. Yu, Z. Lin, G. Zhang, Y. Li, and X. Ran, "A novel Chrysanthemum-like fractal structure multi-band antenna for mobile terminals," *International Journal of RF and Microwave Computer-Aided Engineering*, vol. 2023, Article ID 1102668, 13 pages, 2023.